Geochemistry Geophysics Geosystems G3
AN ELECTRONIC JOURNAL OF THE EARTH SCIENCES
Published by AGU and the Geochemical Society

Article
Volume 8, Number 3
20 March 2007
Q03012, doi:10.1029/2006GC001327
ISSN: 1525-2027

Friction of sheared granular layers: Role of particle dimensionality, surface roughness, and material properties

Matthew Knuth

Department of Geosciences, Pennsylvania State University, 522 Deike Building, University Park, Pennsylvania 16802, USA

Now at Department of Geology and Geophysics, University of Wisconsin-Madison, 1215 West Dayton Street, Madison, Wisconsin 53706, USA (mwknuth@wisc.edu)

Chris Marone

Department of Geosciences, Pennsylvania State University, 522 Deike Building, University Park, Pennsylvania 16802, USA

[1] We report on laboratory experiments designed to investigate three fundamental deformation mechanisms for frictional shear of granular fault gouge: sliding, rolling, and dilation. Mechanisms were isolated by shearing layers composed of rods in geometric configurations that resulted in one-dimensional, two-dimensional, and rolling-only particle interactions. Results of digital video are presented with measurements of friction and strain to illuminate the distribution of shear and the relationship between particle motions and friction. The double-direct-shear configuration was used with boundary conditions of constant layer normal stress (1 MPa) and controlled shear loading rate (10 μm/s) with initial layer thickness of 6 mm. Layers were sheared in a servo-hydraulic testing machine at room temperature (22°C) and relative humidity (5 to 10%). Three materials were studied: alloy 260 brass, dried semolina pasta, and hardwood dowels, with particle diameters of 1.59 mm, 1.86 mm, and 2.06 mm, respectively. Pasta layers had mean sliding friction coefficients of 0.24, 0.11, and 0.02 in 2-D, 1-D, and rolling configurations, respectively. Layers of brass rods had average friction coefficients of 0.23, 0.15, and 0.01, respectively, in 2-D, 1-D, and rolling configurations; and the wood samples exhibited friction values of 0.18, 0.19, and 0.09, respectively. Evolution of strength during shear correlated strongly with the displacement derivative of layer thickness. SEM images document the role of surface finish on frictional properties. Rapid reorientations of particles correspond to stick-slip stress drops and may be related to the collapse and reformation of granular force chains. We find a systematic relationship between the strength of granular layers and (1) the surface roughness of particles and (2) the number of particle contact dimensions. Our data provide important insights on the mechanics of granular fault gouge and constraints on the fundamental parameters used in numerical models of tectonic faulting.

Components: 7756 words, 14 figures, 1 table, 2 animations.

Keywords: granular mechanics; friction; fault gouge.

Index Terms: 0550 Computational Geophysics: Model verification and validation.

Received 6 April 2006; **Revised** 26 July 2006; **Accepted** 6 October 2006; **Published** 20 March 2007.

Knuth, M., and C. Marone (2007), Friction of sheared granular layers: Role of particle dimensionality, surface roughness, and material properties, *Geochem. Geophys. Geosyst.*, *8*, Q03012, doi:10.1029/2006GC001327.

1. Introduction

[2] Fault zones in the upper crust and lithosphere undergo shear via brittle frictional sliding and cataclasis, which generates a wear zone of crushed rock called "fault gouge" [e.g., *Sammis et al.*, 1987; *Scott et al.*, 1994; *Chester et al.*, 2005; *Reches and Dewers*, 2005]. Fault gouge, which can vary in width from tens of cm on young faults to hundreds of m on mature faults [e.g., *Scholz*, 1998], dictates key aspects of fault behavior and earthquake physics, including fault strength, seismic potential, and earthquake properties. For fault zones that cut quartzo-feldspathic rocks of the upper crust, gouge is often dominated by granular material. Thus understanding the physical processes of granular friction is critical to a quantitative interpretation of fault mechanics [e.g., *Scholz*, 1998].

[3] A central problem in fault mechanics and earthquake physics is that of understanding how fault gouge influences the strength and stability of frictional sliding. The mechanical and hydrologic properties of fault gouge are critical parameters in models of frictional heating and thermal pressurization [e.g., *Irwin and Barnes*, 1975; *Mase and Smith*, 1987; *Andrews*, 2002; *Rice*, 2006]. Theoretical works often predict qualitative changes in behavior for relatively minor variations in fault zone properties, and thus detailed laboratory experiments designed to identify and constrain such properties are critical.

[4] Numerical models form a vital link between laboratory experiments and field observations of faulting and tectonic processes. Distinct-Element-Modeling and Finite-Element-Modeling methods have demonstrated the contributions of grain size [*Radjai et al.*, 1996], grain-size distribution, strain rate, and particle collision [*Ketterhagen et al.*, 2005], among other factors. However, limitations in computing power have restricted many of these models to two-dimensional systems. This has led to a disconnect between model results and realistic behavior observed in fault zones and laboratory experiments [e.g., *Mair et al.*, 2002; *Morgan*, 1999; *Mair and Marone*, 1999]. In particular, many existing numerical models predict lower overall macroscopic frictional strength and greater variability in friction as a function of shear of the layer as a whole than corresponding laboratory experimental results [*Mair et al.*, 2002]. At least part of these differences stem from the two-dimensional nature of many early numerical models [e.g., *Hazzard and Mair*, 2003; *Abe and Mair*, 2005].

[5] The purpose of this paper is to report on experiments designed to allow direct comparison with results from two-dimensional numerical simulations and provide constraints on fundamental parameters used in models of tectonic faulting. We shear layers composed of packed cylinders in geometric configurations that resulted in one-dimensional, two-dimensional, and rolling-only particle interactions (Table 1). We use the term "dimensional" here to indicate the degrees of freedom available to individual rods, with rods in the 2-D configuration able to displace in both the shear and normal directions, but with rods in the 1-D configuration able to displace only in the shear direction. The 1-D configuration thus provides a measure of intrinsic friction for interparticle slip.

2. Experimental Technique

[6] Granular layers were deformed in a double-direct shear configuration using a servo-controlled, biaxial testing machine (Figure 1). In this configuration, two identical layers are sheared between three steel forcing blocks (Figure 2). The boundary conditions for our experiments were constant normal stress (1 MPa) and controlled shear displacement rate (10 μm/s). This applied normal stress is in the linear elastic stress range for all three materials used. The outer blocks in the double direct shear configuration are allowed to move normal to the shear direction while the center block is driven downward at constant velocity (Figure 2). For the experiments described here, the contact surface of the outer blocks is 10 cm $\times$ 10 cm and the surfaces of the central block are 15 cm $\times$ 10 cm, 10 $\times$ 10 centimeters of which are in contact with the layer at the beginning of an experiment. Thus the nominal frictional contact of the layer is constant (0.01 m^2) throughout shear. To allow focus on granular deformation mechanisms, without complications due to grain fracture, layers were sheared at a normal stress below the particle fracture strength. Stresses and displacements are recorded continuously at 10 kHz during shear and averaged to 10 Hz for data storage. Normal stress is applied with a high-speed, servo-hydraulic ram and measured to $\pm$0.01 MPa. Displacement measurements are recorded with a precision of $\pm$0.1 μm. It is important to note here that what is measured is only the macroscopic frictional properties of the layer as a whole. The normal and shear stresses at individual particle contacts cannot be determined from our measurements, and may be significantly higher than the far-field stresses.

Table 1. Details of All Experiments

Exp. #	Material	Configuration	Diam., mm	μmean	μstdev	Layer Thick., mm
p347	brass	2-D	1.59	0.239	0.060	5.23
p389	wood	2-D	2.06	0.183	0.026	5.40
p397	pasta	2-D	1.86	0.241	0.013	4.83
p398	pasta	2-D	1.86	0.233	0.022	6.73
p399	wood	2-D	2.06	0.183	0.059	5.43
p405	pasta	1-D	1.86	0.107	0.002	5.23
p406	pasta	1-D	1.86	0.115	0.001	4.68
p413	brass	1-D	1.59	0.150	0.002	5.79
p415	wood	1-D	2.06	0.203	0.001	6.11
p419	brass	1-D	1.59	0.155	0.002	5.79
p420	brass	1-D	1.59	0.147	0.002	6.14
p423	wood	1-D	2.06	0.183	0.002	6.16
p424	pasta	1-D	1.86	0.114	0.001	5.40
p425	wood	2-D	2.06	0.175	0.056	5.32
p426	brass	rolling	1.59	0.013	0.000	5.30
p427	brass	2-D	1.59	0.228	0.049	5.34
p435	wood	rolling	2.06	0.090	0.010	6.59
p436	pasta	rolling	1.86	0.024	0.004	6.33
p451	pasta	2-D	0.85	0.282	0.007	5.27
p452	brass	2-D	1.59	0.251	0.055	6.10
p925	wood	rolling	2.06	0.072	0.009	6.59
p938	brass	rolling	1.59	0.014	0.002	5.24
p939	wood	rolling	2.06	0.077	0.007	7.16
p940	pasta	rolling	1.86	0.018	0.002	5.89

2.1. Granular Materials and Particle Dimensionality

[7] We sheared rods of wood, brass, and pasta (Figure 3) in three configurations designed to produce granular layers that deform via (1) one-dimensional particle interactions, (2) two-dimensional particle interactions, and (3) interparticle rolling only (Figure 4). The choice of materials was made to provide variation in material properties from fused quartz rods used in prior work of a similar nature [e.g., *Frye and Marone*, 2002a, 2002b]. In the 1-D configuration, frictional strength of the sheared layer is determined solely by interparticle sliding. In the 2-D configuration, frictional strength is a sum of rolling, interparticle sliding, and volumetric work of layer compaction and dilation. In the rolling configuration, layers shear solely by rolling between rods.

[8] Rods consisted of dried semolina pasta, alloy 260 brass, and hardwood dowels, with particle diameters of 1.86 mm, 1.59 mm, and 2.06 mm, respectively (Figure 3). In each case, rods were cut to lengths of 10 cm and the ends were polished to remove burrs and imperfections. The materials were chosen to represent a range of surface rough-

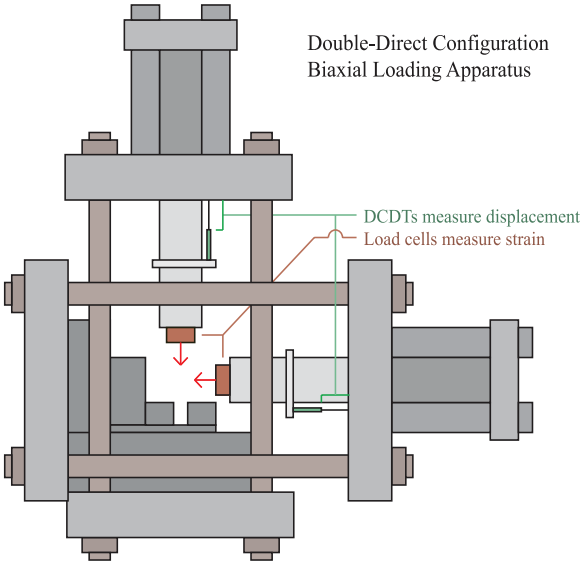

Figure 1. Rough schematic of biaxial loading apparatus. Direct current displacement transducers (DCDTs) measure displacement of both hydraulic rams. Beryllium-copper load cells measure the applied force.

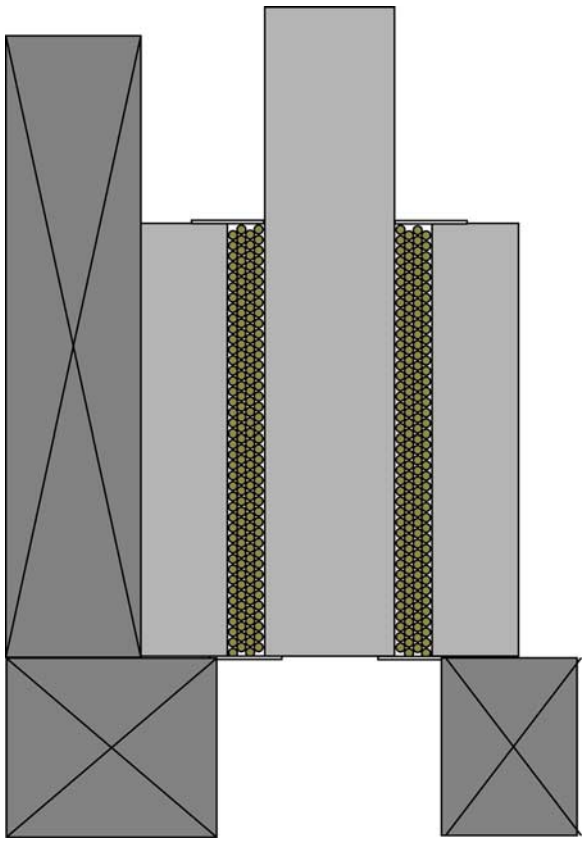

Figure 2. Schematic of sample configuration (2-D). The center forcing block is driven downward in displacement rate servo control by the vertical hydraulic ram. A constant-force boundary condition is applied to the rightmost side block. Large steel support blocks keep the forcing blocks orthogonal to each other and to the frame. Cardstock shims prevent particle escape.

Figure 3. Sample materials clockwise from left to right: #8 semolina pasta (spaghetti), hardwood dowels, and alloy 260 brass rods. Inset: 1 mm fused silica rods granular shear.

ness and hardness (Figure 5). Particle compressibility and breaking strength were measured by subjecting a 10 cm × 10 cm monolayer of rods to uniaxial compression between hardened steel platens. The relationship between particle deformation and applied force was measured for each material over the range 0 to 60 kN; the upper limit of this range corresponds to an average, layer-normal stress of 6 MPa. Wood exhibits plastic deformation at ~30 kN, and pasta exhibits plastic deformation at ~50 kN. Brass deforms elastically through 60 kN of applied force. At 10 kN applied force, which corresponds to the 1 MPa nominal normal stress used in our experiments, percent axial strain was 0.2, 0.28, and 0.44 for brass, pasta, and wood rods, respectively.

[9] SEM imagery documents significant differences in the material surface roughness (Figure 5). Pasta rods are rough and exhibit a scaly texture. Brass rods are smooth but include scratches and other minor imperfections at the micron scale. Wood rods are quite rough and exhibit a fibrous texture at the scale of tens of microns (Figure 5). A limited suite of experiments was conducted using fused quartz rods, which are quite smooth at the micron scale (Figure 5).

2.2. Layer Construction

[10] Granular layers are constructed in a specific sequence to ensure reproducible particle packing and layer characteristics. The 2-D sample config-

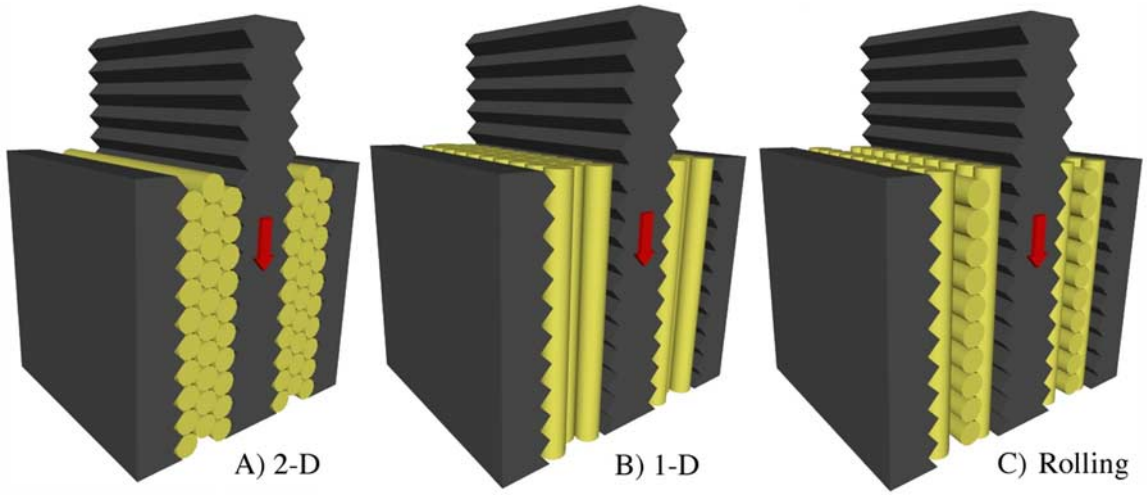

Figure 4. Granular layer configurations. (a) Particles in the 2-D configuration have two degrees of contact freedom. The strength of the layer is a function of interparticle sliding, rolling, and layer dilation. (b) Particles in the 1-D configuration have only one degree of freedom, and friction is a function of the strength of interparticle sliding contacts. (c) Particles in the Rolling configuration have one degree of freedom. Layer strength is a function of friction at rolling contacts and dilation induced by particle eccentricity.

uration is constructed one layer at a time, using precision ground and square blocks as shown in Figure 6. Because the cylinders are the same diameter and constructed carefully, layers are approximately in a closest-packed geometry prior to shearing. This was confirmed by observation of the layers prior to shearing. Layer thickness of the 2-D layers prior to shear ranged from 5 to 6 mm, depending on the number of particle layers and the diameter of the rods (Table 1).

[11] The other sample configurations are built in much the same way. In the 1-D configuration, the rods are rotated 90 degrees so that their long axis is parallel to the shear direction (Figure 4). Because the rods run parallel to the free surfaces on the sides (e.g., Figure 2), guide plates are bolted onto the front and back of the assembly to keep particles from escaping.

[12] To ensure that shear occurs within the layer of particles, the frictional strength of the particle-forcing block contact must exceed that of the interparticle contacts. We ensure that this boundary condition is met by allowing the grooves in the forcing blocks, which are perpendicular to the sample rods, to dig in to the outer particle layer, holding it fixed. This method causes permanent deformation in the outer monolayer of particles, particularly in the wood rods; however, that occurs prior to the application of shear load and post-experiment analysis shows that these deformation grooves do not slip or undergo shear deformation during the experiment. Layer thickness of the 1-D layers prior to shear ranged from 4.7 to 6.2 mm (Table 1). Because the layer is constructed with the particles arranged in a closest-packed configuration, the thickness of the layer is expected to be $2R\,[1 + \cos(30^\circ)\,(n - 1)]$, where R is the particle radius and n is the number of layers. This matches the reported initial layer thicknesses for most experiments ±0.2 millimeters, although gaps in the initial layer or particle escape during compaction may reduce thickness further.

[13] The Rolling configuration is built in the same way as the 1-D configuration but with the central monolayer of particles on either side rotated 90 degrees (Figure 4). The only complication this causes is that the rods in the central layer must be slightly shorter than 10cm so that they do not come into contact with the guide plates. In this configuration, the full layer is always three particles thick, with the total layer thickness dependant only on particle diameter rather than a predetermined target thickness as in the other two configurations. This layer thickness varies over time if the particles are being deformed and their cross section becomes ovoid.

2.3. Shear Test Procedure

[14] Once a normal load was applied, the thickness of the sample was measured to ±0.05 mm. This value varied between experiments (Table 1), however, the precise initial thickness value was used in each experiment to compute volumetric and shear

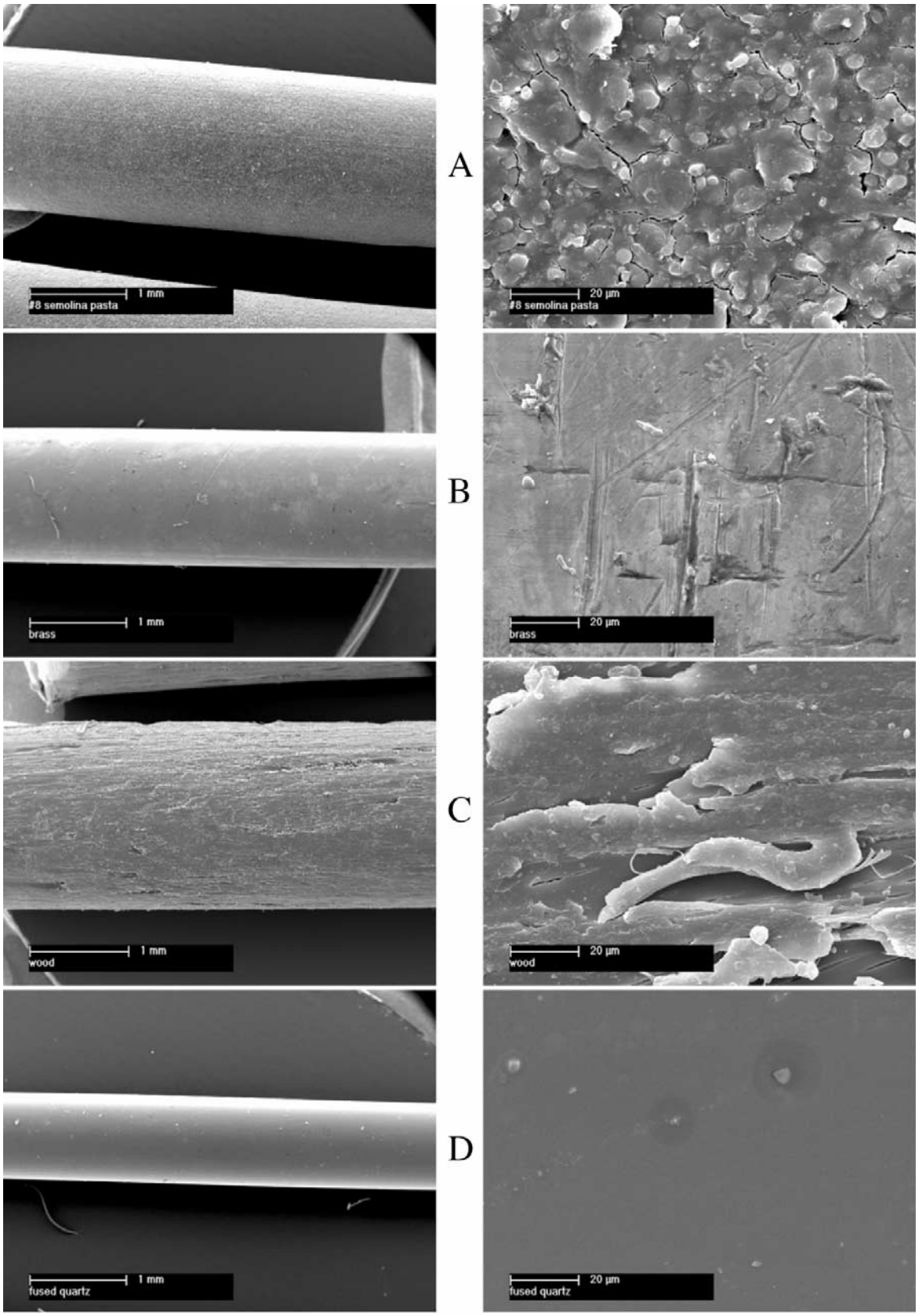

Figure 5. Scanning Electron Microscope imagery of rods: (a) pasta, (b) brass, (c) wood, and (d) fused silica. High-magnification images show marked differences in the surface roughness between materials.

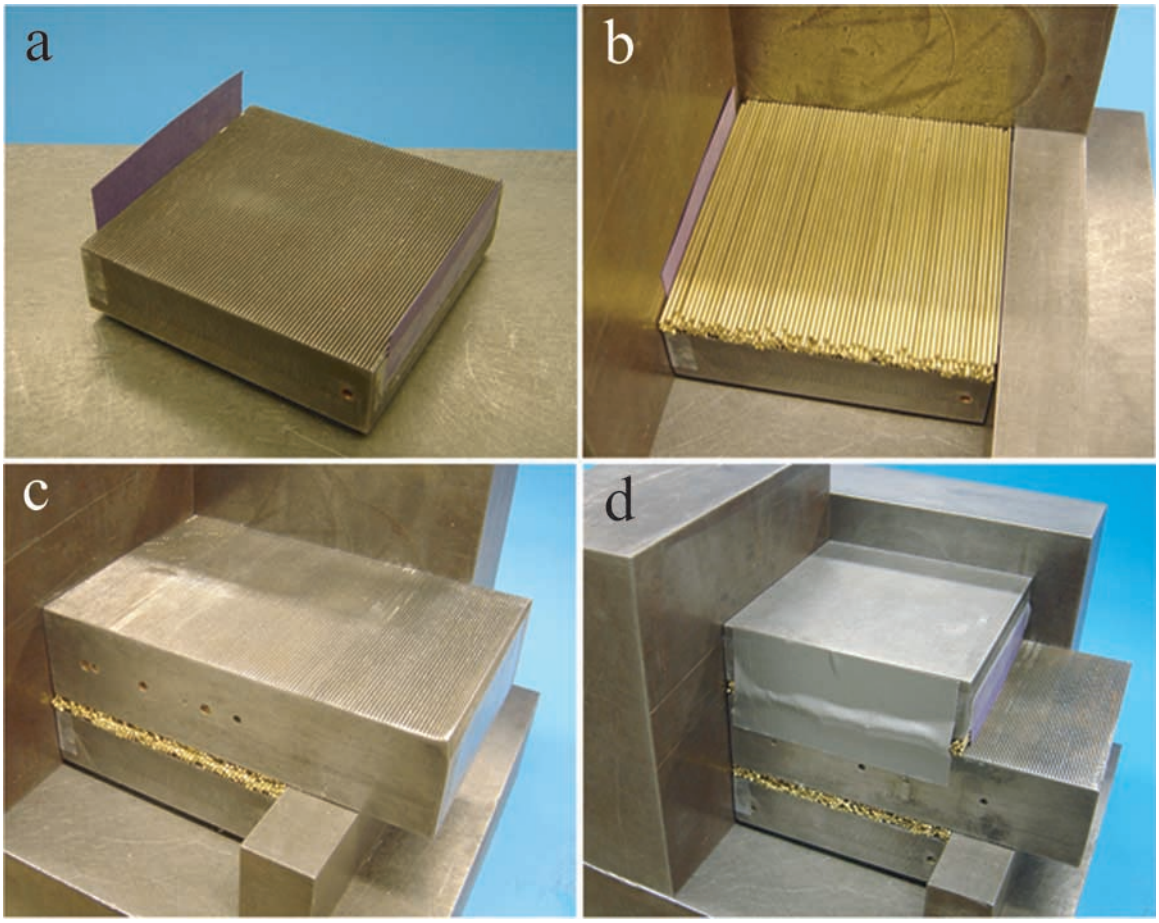

Figure 6. Layer construction. (a) Application of cardstock shims. (b) Filling of first layer. Note that the layer thickness is determined by the height of precision guide block to right. (c) Center block is dropped straight down on layer, using large guide blocks to keep assembly square. (d) Construction of the second layer. Note that the assembly is held together with duct tape until it is brought under normal load.

strain from displacement transducer measurements of slip and layer normal displacement.

[15] Layers are sheared by advancing the vertical ram of the testing machine and displacing the center forcing block (Figure 2) at a constant displacement rate (Animation 1) of 10 microns/second. This load point displacement is maintained to ±0.1 micron by a high-speed servo controller. Because the voltage range of the displacement transducer on the vertical ram (Figure 1) covers less displacement than the experiment requires, it is necessary to perform two "offsets" during the run (Figure 7). These take 10–20 seconds and involve locking the vertical ram in place while repositioning the DCDT core and/or electrically offsetting the output signal. In the data record, the apparent fluctuations in displacement without corresponding changes in the other channels produce sharp spikes in the data. Coupled with concerns about potential healing in the layers during the hold, all statistical calculation were done on only the area between the offsets, excluding the time periods they appear to effect.

[16] Temperature and humidity were not explicitly controlled in this study. The bulk of these experiments (Table 1) were conducted within a period of several weeks over the winter, during which the relative humidity varied from values as low as 7% to values as high as 30%. Temperature in the lab remained consistent at 24–25 degrees Celsius. Humidity has been shown to have an effect on the average coefficient of friction for layers of glass rods [*Frye and Marone*, 2002a], with μ_{mean} increasing by 0.01 between 5 and 30% humidity.

3. Data and Observations

[17] For each experiment, 5 data channels are recorded; vertical and horizontal displacement, normal and shear load, and an average sampling interval

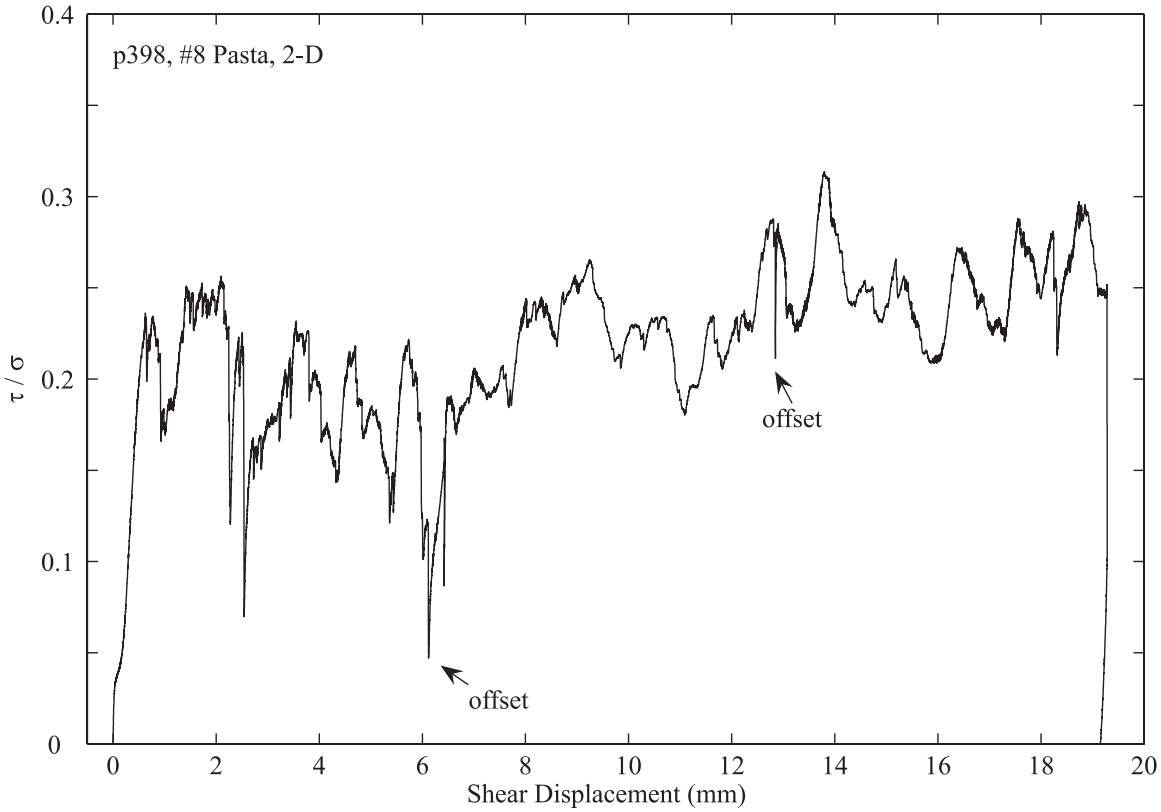

Figure 7. Friction data for a typical experiment run in the 2-D configuration. μ, the ratio of shear stress τ to normal stress σ, is plotted on the y axis. Because the displacement rate was a constant 10 microns/second, 2 mm along the x axis is equivalent to 200 seconds. The arrows indicate the two transducer voltage offsets, at which point shearing is halted for 5–10 seconds.

(10 Hz). Shear and normal displacements are corrected for elastic deformation of the apparatus, using values obtained in detailed calibrations. The true sample boundary displacement is used to calculate shear and volumetric strain in the layer. The voltage signals from the load cells are converted into stresses using the known area of the sample blocks and the calibration values of the load cells. The coefficient of friction μ for the layer is calculated by dividing the shear stress by the normal stress (Table 1).

3.1. Two-Dimensional Configuration

[18] We plot the normalized shear strength (coefficient of friction) against shear displacement to illustrate the variation in macroscopic frictional strength over the course of an experiment (Figure 7). The first-order behavior exhibited in Figure 7, is typical of all experiments and includes an initial elastic stress increase, followed by inelastic yield at 5.6% strain and then fully mobilized frictional shear. For the 2-D experiments, inelastic yield occurs at shear displacements of 0.3–0.5 mm, which correspond to shear strains of 5–8%. Determining the precise transition from elastic loading to inelastic shear is complicated by dilation effects, especially in the wood layers. The macroscopic frictional strength of the 2-D layer varies considerably with shear, ranging from 0.1 to 0.25 (Figure 7). The two vertical displacement offsets are indicated in Figure 7. Note that shear stress decreases during these intervals due to creep. The effect on strength of the ''offsets'' depends on the degree to which the short pause permits frictional restrengthening, and is generally minimal compared to natural strength variations in the 2-D configuration. The holds are equivalent to slide-hold-slides conducted to study healing in prior experiments [*Frye and Marone*, 2002a], albeit on the order of only a few seconds. With continued shear, we often observed a gradual strengthening and a reduction in the variance of friction (Figure 7).

[19] Both the magnitude of μ and its variance throughout an experiment change in a reproducible way between configurations and between materials run in the same configuration (Figure 8). Wood rods produce a long-wavelength, smooth variation. Their first-order behavior is characterized by oscillations in μ on the order of 0.2, while second-order

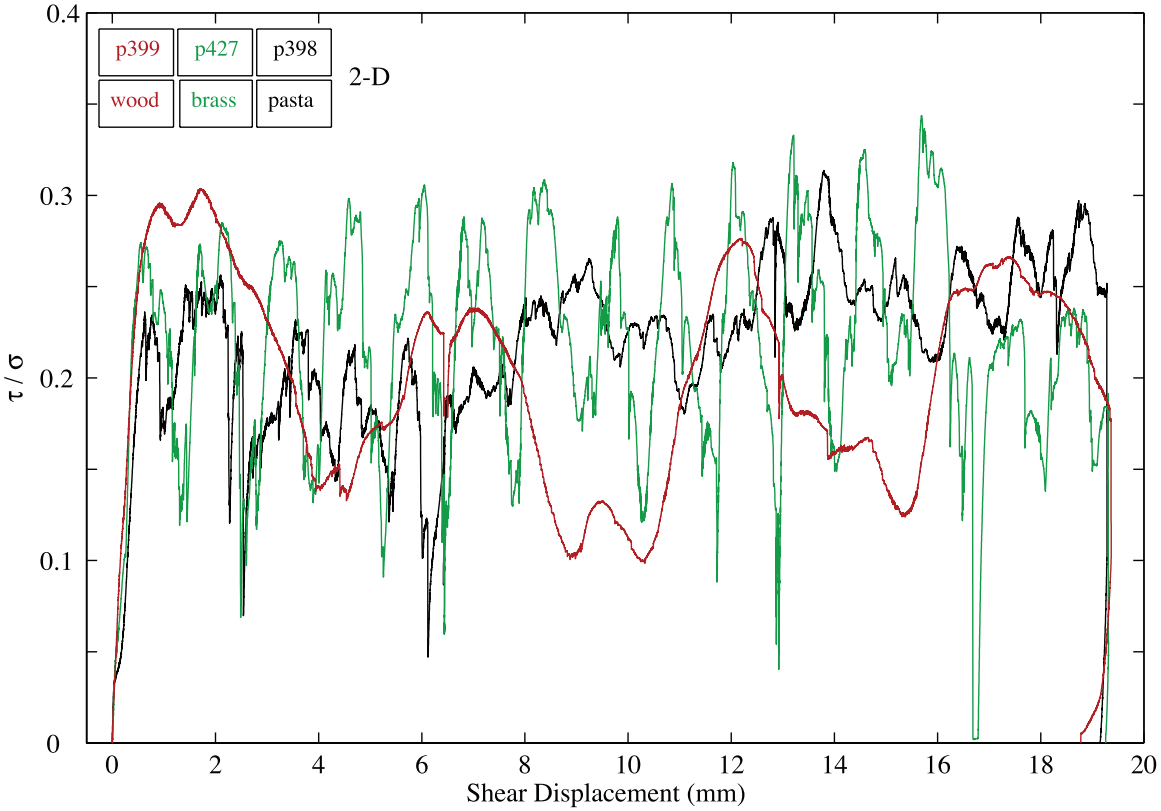

Figure 8. Comparison of granular materials in the 2-D configuration. Wood layers exhibit long wavelength, smooth variations. Pasta and brass exhibit higher-frequency variation. In all cases, sliding is stable and without abrupt, audible stick-slips.

fluctuations of about 0.02 are evident in the local minima and maxima.

[20] The pasta rods do not show the same long-wavelength oscillations as the wood rods. Instead, the coefficient of sliding friction for pasta rods increases gradually while undergoing second-order oscillations that range in (friction) magnitude from 0.01 to 0.05 and wavelength of 0.03 to 1 mm.

[21] The brass rods show roughly the same second-order variation as the pasta, with variations on the order of three cycles per four millimeters of displacement. The magnitude of these oscillations is much larger, and as with wood is on the order of 0.2 in friction. Unlike the pasta rods, the brass rods do not exhibit a gradual strengthening with net displacement, although the magnitude and wavelength of the oscillations in μ are much more consistent over the course of the experiment. The brass exhibits the same irregular second-order variations as the pasta.

3.2. One-Dimensional Configuration

[22] For all three materials run in the 1-D configuration, μ peaks during the initial onset of shearing, and then falls off to a relatively constant value (Figure 9). Small spikes and brief periods of noise in these experiments are associated with the very low values of resolved shear stress, low enough in some cases to approach the background noise levels of the load cells. The evolution of μ with slip varies between materials. Wood layers weaken with slip throughout the entire experiment, although the decrease is small. In contrast, brass rods weaken slightly after the initial peak strength, but this persists for only ~500 microns before strengthening begins. The pasta layers decrease in strength during the first 5–6 mm of slip, but then slip without appreciable change in strength beyond that. All three materials exhibit strength drops of similar magnitude following shear-displacement holds, suggesting some degree of creep during the time the layer is stationary. Both the evolution of friction over time and the overall strength of each material were consistent between different experiments run on the same material (Table 1).

3.3. Rolling Configuration

[23] The strength of experiments run in the rolling configuration is lower than the 1-D and 2-D con-

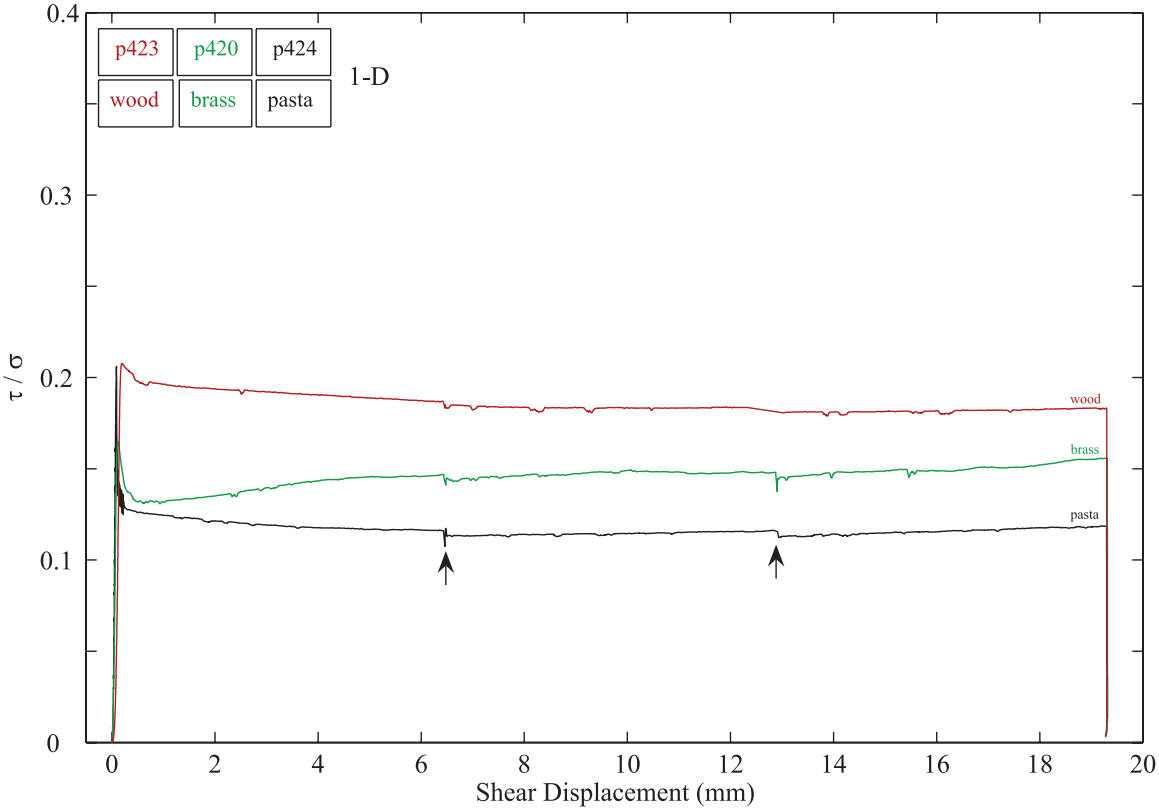

Figure 9. Comparison of materials in the 1-D granular configuration. Wood layers are consistently the strongest and exhibit a distinct peak on initial loading. The brass layers exhibit a more pronounced peak strength and slip-hardening. Arrows note the positions of the pauses in shearing resulting from transducer voltage offsets.

figurations and varies sinusoidally over the course of the experiment. Strength oscillations in rolling experiments vary in amplitude and wavelength between the three materials (Figure 10). The brass rods exhibit a constant μ of 0.015 ± 0.01. There is no initial stress peak such as that seen in the 1-D experiments, and even the pauses in the experiment for the vertical offsets produce little variation. The frictional coefficient of pasta rods varies between 0.2 and 0.3 in a regular, sinusoidal pattern with wavelength of 6.6 mm. Layers of wooden rods are much more resistant to displacement in this configuration, with μ averaging around 0.1 with much higher variance than brass or pasta. The coefficient of friction in the layer exhibits the same regular oscillation seen in the pasta rods, but with a slightly longer wavelength of 7.5 mm.

3.4. Digital Imaging of Layer Deformation

[24] To provide additional constraints on the micromechanics of granular shear, several of the 2-D experiments were recorded using a digital video camera (Animation 2). In the 2-D configuration, rod ends are visible from the side. This provides an opportunity to observe strain localization in situ. The ends of the brass rods were painted to provide strain indicators, and the video in Animation 2 is sped up by a factor of 125. We constructed synchronized plots of the measured frictional strength, layer thickness, and changes in layer thickness to illustrate their relationship with particle motion and interparticle interactions (Animation 2). The sound channel from the digital video has been filtered to remove machine noise. The remaining signal includes audible pops associated with stick-slip and rapid reorientation of particles within the layer. The louder events correspond to distinct drops in frictional stress and, generally, layer compaction events (Animation 2).

3.5. Particle Motions

[25] Comparing the instantaneous geometry of the layer to its frictional state allows us to assess the role of particle arrangement in determining the strength of the layer, through jamming and networked force distribution. Previous studies conducted on flat disks in a ring-shear apparatus have imaged these factors using photoelastic materials

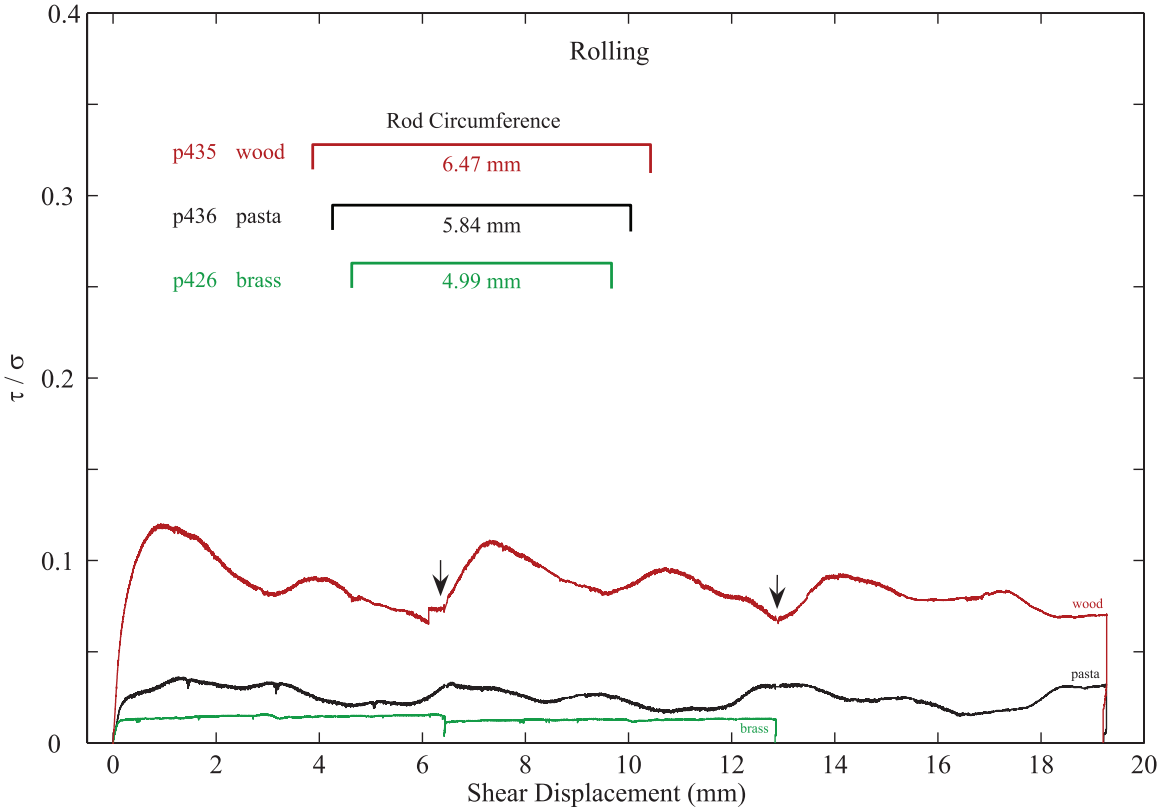

Figure 10. Comparison of materials in the Rolling granular configuration. Wood is the strongest and exhibits the largest variations. The wavelength of the fluctuations for wood and pasta is similar to the particle circumference. Arrows again note the positions of the pauses in shearing resulting from transducer voltage offsets.

[e.g., *Hartley and Behringer*, 2003; *Majmudar and Behringer*, 2005]. These studies indicate that stress transmission in a granular layer is accomplished through the formation and destruction of "force chains," which consist of an anastamosing network of contacting particles that extend between the layer boundaries. Interparticle contact forces are high for particles within a force chain and significantly lower for "spectator" particles in intervening regions. The arrangement of these chains at any point in time determines which sections of the layer are "jammed" and which sections are free to deform through sliding or rolling [*van Hecke*, 2005]. Force chains have been explored in recent work through both numerical modeling [e.g., *Aharonov and Sparks*, 2002; *Taboada et al.*, 2005; *Fortin and Coorevits*, 2004] and laboratory experiments [e.g., *Stone et al.*, 2004].

3.6. Analysis of Experimental Results

[26] Mean values for μ are calculated using the portion of each experiment between the two vertical displacement offsets (Figure 11, Table 1). In general, mean friction increases linearly as a function of the degree of freedom available to individual particles (Figure 11). Data for fused quartz rods are taken from *Frye and Marone* [2002a]. Pasta and brass rods display a simple linear increase in frictional strength with particle dimensionality, if we assign rolling to a zero-degree frictional process. The wood rods behave somewhat differently, exhibiting high values of frictional strength in the rolling configuration and lower 2-D friction compared to 1-D friction. These observations are consistent with higher tensile contact strength for wood, due to its fibrous surface texture. Because the grain of the wood runs parallel to the rods, the interaction between long features on the surface is not relieved through shear in the 1-D configuration, whereas rolling provides a mechanism to break these contacts in the 2-D and rolling configurations.

4. Discussion

[27] Friction is often characterized as a surface property, but frictional strength of a granular layer and its variations with slip rate and sliding history also depend on bulk material properties [e.g., *Rabinowicz*, 1956; *Bowden and Tabor*, 1964].

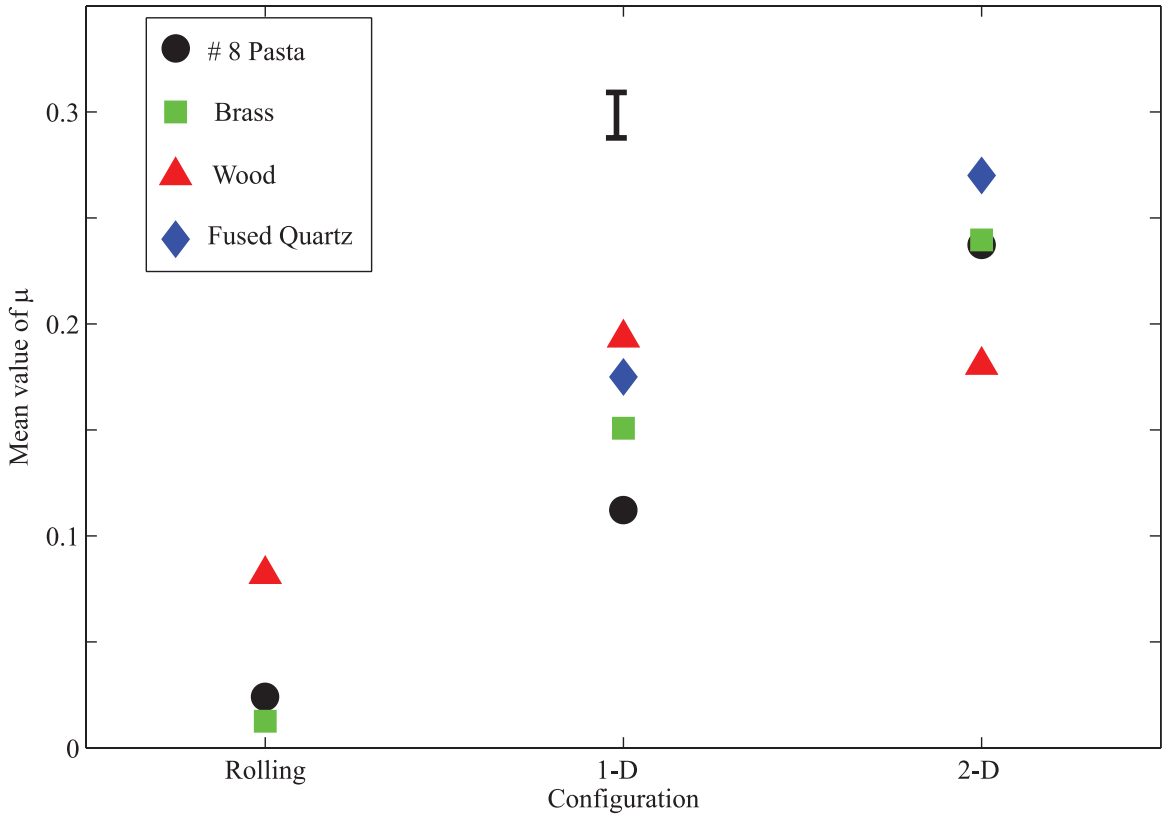

Figure 11. Mean coefficient of friction as a function of granular shear configuration. Uncertainty in friction is on the order of ±0.01. Each point represents an average of a subset of experiments. Frictional strength varies systematically with degrees of freedom in granular shear. Data for fused quartz rods are taken from *Frye and Marone* [2002a].

Our data provide constraints on the fundamental parameters used in numerical models of tectonic faulting and important insights into the mechanics of granular fault gouge.

[28] Four basic properties define the difference between particles used in our experiments. Two of these are experimentally controlled variables and two are variables related to geometric consistency of the particles. Control variables include particle surface properties and elastic properties, which determine deformation style and compressibility. Surface properties include both roughness of the particle surfaces (Figure 5) and physiochemical properties that affect the strength of contact junctions. Elastic properties and strength determine the work done in viscoelastic deformation of particles during shear.

[29] The variables of consistency in our experiments include particle shape and diameter, which varied significantly between the materials. Brass rods are machined to a tolerance of 0.001" (25 μm), whereas the diameter of pasta rods and wood dowels vary along the length of a rod, and between rods, by up to ±200 microns. Variations in particle diameter result in differences in packing geometry and particle coordination number during granular shear. Brass rods are also much more nearly circular in section than pasta and wood rods. Differences in eccentricity couple with differences in compressibility and result in differences in the amount of elastic work done, as well as differences in packing geometry and particle coordination number. The specific contribution of these variables bears further study, but is here assumed to be minimal in comparison to the control variables discussed in the previous section.

4.1. Dilation

[30] Experiments run in the 2-D configuration, particularly those run on wood, show a strong relationship between layer thickness and the coefficient of friction (Figure 12). The record shown in Figure 12 includes layer compaction during application of normal load prior to shear. During shear, we find that frictional strength is high when the layer is dilating from its closest-packed arrange-

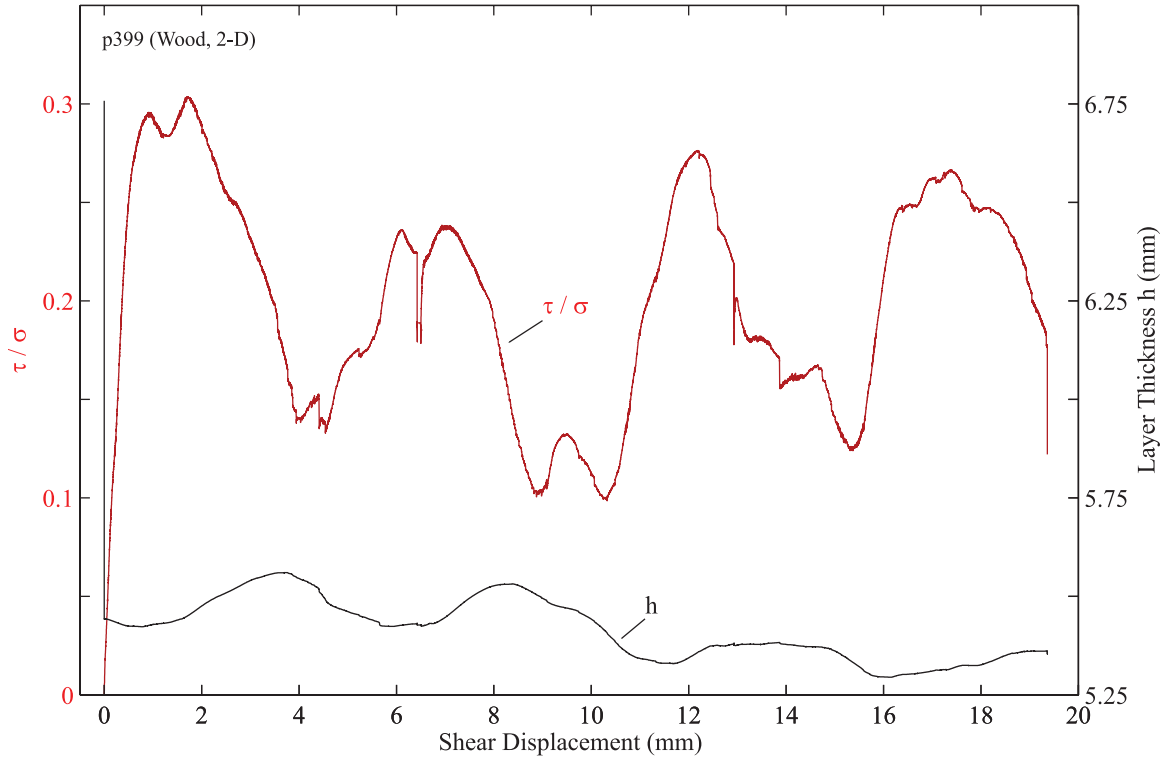

Figure 12. Relationship between layer thickness and friction for a 2-D experiment on wood rods. The upper line in Figure 12 is the coefficient of friction μ, and the lower line is the layer thickness plotted as a function of shear displacement. Friction varies with slip in concert with layer thickness changes and is highest when the layer is dilating.

ment, and lower during compaction (Figure 12). These observations are consistent with previous work showing a connection between granular frictional strength and the rate of dilation (compaction) with shear [e.g., *Bishop*, 1954; *Edmond and Paterson*, 1972; *Frye and Marone*, 2002a].

[31] Quantitative analysis shows that the coefficient of friction varies linearly with the dilatancy rate, which is the derivative of layer thickness, dh, with shear displacement dx (Figure 13). We determined the dilatancy rate dh/dx using a running averaging best fit to the digital measurements of dh and dx. To reduce the effects of noise, we explored a range of window sizes for all experiments and found that ~249 points produced an appropriate balance between over-smoothing and exaggeration of noise and localized behavior. This window corresponds to approximately 25 seconds in time or 250 microns of shear displacement.

[32] The connection between μ and dh/dx can be shown from a simple force balance, given by

$$\tau = \sigma\left(\mu_p + d\phi/d\gamma\right), \quad (1)$$

where ϕ is volume strain, γ is shear strain, and σ is the normal stress. To reduce this into measured quantities, we take $d\phi$ = dV/V, and $d\gamma$ = dx/h where V is sample volume. Volume strain for the thin layers used in our experiments is $d\phi$ = dh A/A h, where A is the nominal frictional contact area, and thus $d\phi/d\gamma$ = (dh A/A h)/(dx/h), which reduces to dh/dx. Equation (1) then becomes

$$\tau = \sigma\left(\mu_p + dh/dx\right), \quad (2)$$

which can be written in terms of the measured frictional strength, μ_{total} as

$$\mu_{total} = \mu_p + dh/dx. \quad (3)$$

[33] The relationship between friction and dilatancy rate is seen consistently in the 2-D experiments, but not in the 1-D experiments. This is to be expected, as the 1-D layer involves only interparticle sliding, which does not require changes in layer thickness. There is some relation between friction and layer thickness in the Rolling configuration, which may reflect elastic deformation and eccentricity of particles.

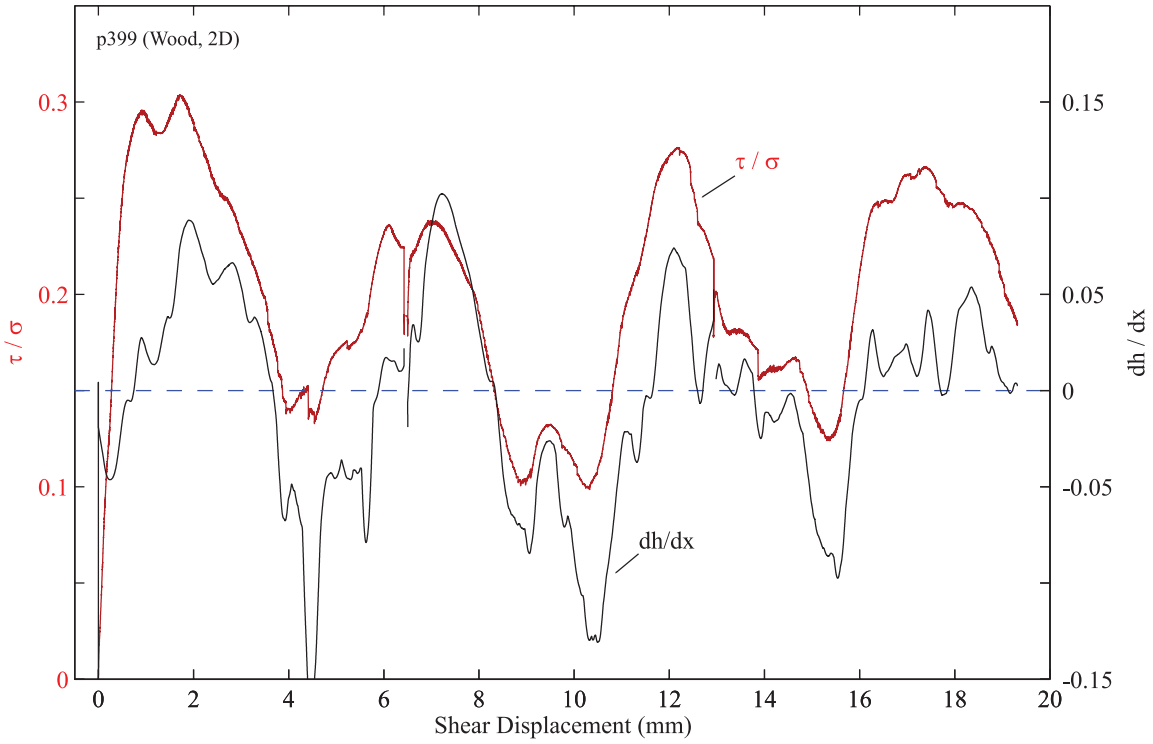

Figure 13. Plot of the same experiment shown in Figure 12 showing the relationship between μ and the dilatancy rate dh/dx as a function of shear displacement. Note the strong correlation between frictional strength and dilatancy rate.

[34] The inter-particle contact friction, μ_p, determined using the offset between dh/dx and μ_{total}, is 0.15 for the experiment described by Figure 13, which is of similar magnitude to that predicted by the 1-D experiments on wood. In this case, the lower contribution of interparticle friction in the 2-D configuration may be a function of the anisotropy in the surface of the wood rods.

[35] The strength of the correlation between dh/dx and the coefficient of friction varies between configurations and materials (Figure 14). A value of 1 in Figure 14 would indicate perfect linear correlation, with values of 0 suggesting no significant correlation and −1 being perfect anti-correlation. The groupings of material and configuration are consistent, implying that this is a reproducible behavior. The 1-D experiments plot around 0 or as negative values. In the rolling configuration, the effects of dilatancy vary with the expected cross-sectional eccentricity of rods, with wood being the highest and brass lowest.

4.2. Sliding

[36] Our 1-D configuration is theoretically the simplest; as frictional strength should vary only with physiochemical surface properties. Granular layers of "1-D" particles do not have to dilate to accommodate particle displacement, and there should be no force exerted across the cross-section of the rods in an orientation that would induce them to roll. The strength of the layer is therefore determined only by resistance to inter-particle sliding.

[37] It is interesting to evaluate variations in frictional strength as a function of net shear (Figure 9). The pasta and wood layers gradually weaken after the initial peak strength, flattening out to a slow decline. The brass rods have the same high initial peak and failure, but the layer continues to strengthen over the remainder of the experiment. This disparity implies that surfaces differ in more than just the number of asperities. The inter-particle contacts also evolve differently between materials. With this in mind, the differences among the materials in 1-D may best be explained through examination of SEM images of their respective surfaces.

[38] The surfaces of quartz rods used in prior studies [*Frye and Marone*, 2002a, 2002b; *Anthony and Marone*, 2005] are characterized by small circular globules (Figure 5). These imperfections account for less than 1% of the total surface area.

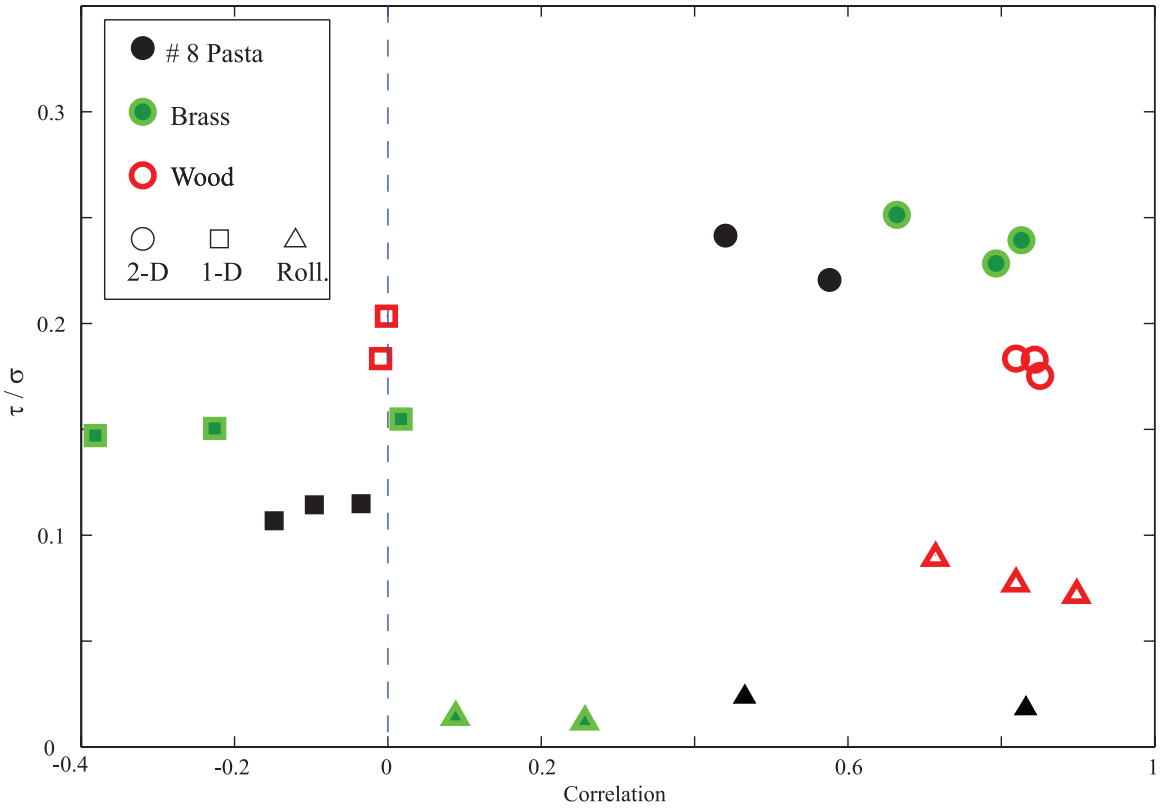

Figure 14. Scatterplot of linear correlation coefficient against the coefficient of friction for all experiments. Experiments in the same configuration and with the same material plot in the same general area, suggesting good reproducibility of results. Correlation strength in the rolling configuration is a function of particle eccentricity.

The remainder of the rod's surface appears completely smooth. Fresh rods of pasta are characterized by an irregular network of desiccation cracks and starch nodules. The cracks are on the order of one micron in width. The starch nodules range from 10–20 square microns in area and are less than 20 microns in height. Images of the pasta after an experiment did not show these cracks. We typically observed very fine dust after experiments with pasta experiment, which is consistent with wear of these starch nodules.

[39] Figure 5 shows the surface of a brass rod after shearing. It is characterized by deep gouges that are ~2 microns in width (Figure 5). These do not appear on the surface of fresh rods, which are featureless. The wear grooves visible in Figure 5 are oriented parallel to the long axis of the cylinder or on a plane orthogonal to it. The latter were generated by experiments run in the 2-D or rolling configurations, while the former were formed at sliding contacts in the 1-D configuration. The mechanism for creating these gouges could be spalling, interaction between asperities, or some combination of the two. A large amount of adhesion and spalling should increase the coefficient of friction over time [*Bowden and Tabor*, 1964], which is consistent with observations from the 1-D experiments (Figure 9). There was no apparent residue left behind from damage to the brass rods during shear.

[40] The surface of the wood rods is characterized by deep hollows and fibrous surface projections on the order of hundreds of square microns (Figure 5). Many of these features are roughly linear, oriented with the grain of the wood. This orientation is to be expected, because dowels are manufactured by cutting the wood parallel to its grain. During shear of wood rods, surface fibers become interlocked and must be detached or torn, which contributes to the high friction values observed in the 1-D configuration.

4.3. Rolling

[41] The variations in friction in the rolling configuration reflect a different set of processes than those in the other configurations. With only a single layer actually being strained in this geometry, there is no need for any reordering of particles to accommodate slip. The long, periodic changes in

strength as a function of slip (Figure 10) must be due to some other property. Surface roughness is an unlikely candidate, as it is improbable that every cylinder would be similarly anisotropic. The circumference of the wood rods is 7.4 mm, and the circumference of the pasta rods is 6.9 mm, corresponding to their oscillation wavelengths of 7.5 and 6.6 millimeters, respectively. The similarity between oscillation wavelength and particle circumference confirms that the rods in the layer are rolling, and also implies that the pasta and wood rods are not perfectly cylindrical. The strength of the layer is tied to changes in its thickness, which is in turn tied to the eccentricity of the rolling particles. Because this behavior characterizes the layer as a whole, individual rods must either align themselves during initial loading, with the major axis of their ovoid cross-section perpendicular to the normal stress, or else the loading itself deforms the particles in a way that is not recoverable at the rate at which the layer is sheared. In an ideal case, the thickness of a layer of rolling ellipses will vary as a sine wave between the semi-major and semi-minor axes. This is consistent with the observation that frictional strength varies with the derivative of the layer thickness (Figure 14), although the correlation is weaker, as expected, than that observed for the 2-D configuration.

[42] In a simple model of a rolling ovoid, we would expect two peaks of equal height in a full rotation; with the minima occurring just as the semi-major axis of the particles aligns with the normal stress direction. What we observe is that the first peak is significantly higher than the second (Figure 10). This may represent one of two things. Either the arrangement of the particles becomes disturbed such they do not all share the same alignment, or else the layer is deforming as it rolls. More perfectly cylindrical particles, as evidenced by the brass rods, should exhibit minimal variation in friction when rolling. The fact that the variation in the strength of the wood rods decreases over time may imply that the wood rods are loosing their eccentricity as they roll. This issue could be explored in future work by introducing slide-hold-slide steps into the rolling experiment or by varying the strain rate and normal stress throughout.

[43] Rolling friction can be attributed to several processes, although some of them will only act on spheres [*Bowden and Tabor*, 1964]. Some strength will come from the work necessary to overcome weak inter-particle attraction at the contact interface. Some will also come from work done in the deformation of the contact surface, and some will come from hysteresis associated with particle deformation. In a true 3-D configuration composed of spheres, contact deformation will result in an anisotropic sense of relative velocity over the total contact area, which may result in some degree of sliding [*Bowden and Tabor*, 1964]. For rolling cylinders, some degree of interparticle slip will occur at contact junctions prior to and during rolling. These processes will be exacerbated by surface asperities and by any time-dependant deformation that acts to increase the area of the contact.

[44] A packed layer of rolling particles will have an additional source of sliding friction related to the contact between adjacent particles in front and behind. In our experiments, the in-plane force on these contacts is indeterminate, although elliptical particles would come into stronger contact when their semi-major axis is perpendicular to the normal stress. The stress at these contacts will be highest when the layer thickness is narrowest, so any contribution to frictional strength from these sliding contacts will add to that generated at the rolling contacts.

4.4. Applicability to Fault Mechanics

[45] Determining the relative contribution of rolling and sliding to friction between two adjacent cylinders in the 2-D configuration is impossible using only macroscopic stress/strain measurements and difficult even with the video recordings of strain. Computer models have proven to be extremely useful in this regard, and indicate that rolling contacts are especially important in determining patterns of strain localization and distribution [*Morgan and Boettcher*, 1999]. The surface properties of synthetic materials are difficult to compare directly with those of natural fault gouge material. They are, however, directly applicable to numerical approaches that address questions about the formation, strength, and properties of active fault zones.

[46] Experiments such as those described here provide physical insight and input parameters for numerical models of tectonic processes. In detail, the elastic modulus of brass is higher than that of a typical granite, while the elastic modulus of most hardwood is comparable to that of a weak sandstone. Semolina pasta falls somewhere in the middle, as does fused quartz. Conducting granular friction tests in the lab on a range of different materials with diverse properties thus allows the results to be correlated with a wider range of parameters in the numerical models,

calibrating them to represent actual fault rock more precisely.

[47] The nature of the interparticle surface contacts for different materials provides another way to explore the parameter space of the model. The brass surfaces describe a case where surface interactions are dominated by metallic adhesive processes [*Bowden and Tabor*, 1964], while friction between wood rods is dominated by surface asperity interactions and semolina pasta by a combination of asperity interactions and sub-gouge formation from their brittle outer surfaces. The examination of these more extreme cases provides insight into the more heterogeneous processes acting in a natural fault zone. One could apply our results more directly by scaling the relative effects of adhesion, cohesion, asperities, and sub-gouge formation (e.g., spalling) in a model for macroscopic frictional strength, although that is beyond the scope of this study.

5. Conclusions

[48] We show that material properties and surface characteristics of particles have significant effects on the frictional strength of granular layers. Differences between experimental configurations are exploited to isolate the role of strain accommodation mechanisms in granular layers. The frictional strength of 2-D granular layers varies in a reproducible manner predicted by 2-D computer modeling. We observe that particle deformation style plays a role in determining the shape and periodicity of these variations. Experiments run in the 1-D configuration exhibit negligible variation in strength with slip, which is consistent with pure sliding behavior. Variations in the rolling experiments scale with particle compressibility and eccentricity. Experiments on pasta and brass confirm the roughly linear increase in mean frictional strength with particle-dimensionality and degrees of particle freedom observed by *Frye and Marone* [2002a]. We also observe the same linear correlation between changes in layer thickness and the frictional strength of layers run in the 2-D configuration. The strength of this correlation varies between materials in a consistent and reproducible way, implying that it is affected by material properties, with dilatancy in the layer impacted by particle eccentricity and elasticity. Future work will include a detailed analysis of videos of experiments run in the 2-D configuration in order to elucidate changes in the layer geometry and also the use of different types of materials to expand the range of parameters available.

Acknowledgments

[49] This work has been funded by National Science Foundation grants EAR 0196570, OCE 0196462, and EAR-0337627.

References

Abe, S., and K. Mair (2005), Grain fracture in 3D numerical simulations of granular shear, *Geophys. Res. Lett.*, *32*, L05305, doi:10.1029/2004GL022123.

Aharonov, E., and D. Sparks (2002), Shear profiles and localization in simulations of granular materials, *Phys. Rev. E*, *65*, 051302, doi:10.1103/PhysRevE.65.051302.

Andrews, D. J. (2002), A fault constitutive relation accounting for thermal pressurization of pore fluid, *J. Geophys. Res.*, *107*(B12), 2363, doi:10.1029/2002JB001942.

Anthony, J. L., and C. Marone (2005), Influence of particle characteristics on granular friction, *J. Geophys. Res.*, *110*, B08409, doi:10.1029/2004JB003399.

Bisho, A. W. (1954), Correspondence, *Geotech*, *4*, 43–45.

Bowden, F. P., and D. Tabor (1964), *The Friction and Lubrication of Solids Part II*, Oxford Univ. Press, New York.

Chester, J. S., F. M. Chester, and A. K. Kronenberg (2005), Fracture surface energy of the Punchbowl fault, San Andreas system, *Nature*, *437*, 133–136, doi:10.1038/nature03942.

Edmond, J. M., and M. S. Paterson (1972), Volume changes during the deformation of rocks at high pressures, *Int. J. Rock Mech. Min. Sci.*, *9*(2), 161–182.

Fortin, J., and P. Coorevits (2004), Selecting contact particles in dynamics granular mechanics systems, *J. Comp. Appl. Math.*, *168*, doi:10.1016/j.cam.2003.05.025.

Frye, K. M., and C. Marone (2002a), The effect of particle dimensionality on Granular friction in laboratory shear zones, *Geophys. Res. Lett.*, *29*(19), 1916, doi:10.1029/2002GL015709.

Frye, K. M., and C. Marone (2002b), Effect of humidity on granular friction at room temperature, *J. Geophys. Res.*, *107*(B11), 2309, doi:10.1029/2001JB000654.

Hartley, R. R., and R. P. Behringer (2003), Logarithmic rate dependence of force networks in sheared granular materials, *Nature*, *421*, 928–930, doi:10.1038/nature01394.

Hazzard, J. F., and K. Mair (2003), The importance of the third dimension in granular shear, *Geophys. Res. Lett.*, *30*(13), 1708, doi:10.1029/2003GL017534.

Irwin, W. P., and I. Barnes (1975), Effects of geological structure and metamorphic fluids on seismic behavior of the San Andreas fault system in central and northern California, *Geology*, *3*, 713–716.

Ketterhagen, W. R., J. S. Curtis, and C. R. Wassgren (2005), Stress results from two-dimensional granular shear flow simulations using various collision models, *Phys. Rev. E*, *71*, 061307, doi:10.1103/PhysRevE.71.061307.

Mair, K., and C. Marone (1999), Friction of simulated fault gouge for a wide range of velocities and normal stresses, *J. Geophys. Res.*, *104*(B12), 28,899–28,914.

Mair, K., K. M. Frye, and C. Marone (2002), Influence of grain characteristics on the friction of granular shear zones, *J. Geophys. Res.*, *107*(B10), 2219, doi:10.1029/2001JB000516.

Majmudar, T. S., and R. P. Behringer (2005), Contact force measurements and stress-induced anisotropy in granular materials, *Nature*, *435*, 1079–1082, doi:10.1038/nature03805.

Mase, C. W., and L. Smith (1987), Effects of frictional heating on the thermal, hydrologic, and mechanical response of a fault, *J. Geophys. Res.*, *92*(B7), 6249–6272.

Morgan, J. K. (1999), Numerical simulations of granular shear zones using the distinct element method: 2. Effects of particle size distribution and interparticle friction on mechanical behavior, *J. Geophys. Res.*, *104*(B2), 2721–2732.

Morgan, J. K., and M. S. Boettcher (1999), Numerical simulations of granular shear zones using the distinct element method: 1. Shear zone kinematics and the micromechanics of localization, *J. Geophys. Res.*, *104*(B2), 2703–2720.

Rabinowicz, E. (1956), Stick and slip, *Sci. Am.*, *194*, 109–118.

Radjai, F., M. Jean, J. Moreau, and S. Roux (1996), Force distributions in dense two-dimensional granular systemsPhys. Rev. Lett., 77(2), 274–277, doi:10.1103/PhysRevLett.77.274.

Reches, Z., and T. A. Dewers (2005), Gouge formation by dynamic pulverization during earthquake rupture, *Earth Planet Sci. Lett.*, *235*(1–2), 361–374.

Rice, J. R. (2006), Heating and weakening of faults during earthquake slip, *J. Geophys. Res.*, *111*, B05311, doi:10.1029/2005JB004006.

Sammis, C., G. King, and R. Biegel (1987), The kinematics of gouge formation, *Pure Appl. Geophys.*, *125*(5), 777–812, doi:10.1007/BF00878033.

Scholz, C. H. (1998), Earthquakes and friction laws, *Nature*, *391*, 37–42.

Scott, R. S., D. A. Lockner, J. D. Byerlee, and C. G. Sammis (1994), Triaxial testing of Lopez fault gouge at 150 MPa mean effective stress, *Pure Appl. Geophys.*, *142*(3/4), doi:10.1007/BF00876063.

Stone, M. B., R. Barry, D. P. Bernstein, M. D. Pelc, T. K. Tsui, and P. Schiffer (2004), Local jamming via penetration of a granular medium, *Phys. Rev. E*, *70*, doi:10.1103/PhysRevE.70.041301.

Taboada, A., K.-J. Chang, F. Radjaï, and F. Bouchette (2005), Rheology, force transmission, and shear instabilities in frictional granular media from biaxial numerical tests using the contact dynamics method, *J. Geophys. Res.*, *110*, B09202, doi:10.1029/2003JB002955.

van Hecke, M. (2005), Granular matter: Tale of tails, *Nature*, *435*, 1041–1042, doi:10.1038/4351041a.